Evaluation of Campbell diagrams for vertical hydropower machines supported by Tilting Pad Journal Bearings

Florian Thiery, Rolf Gustavsson, Jan-Olov Aidanpää

Evaluation of Campbell diagrams for vertical hydropower machines supported by Tilting Pad Journal Bearings

Florian Thiery[1]*, Rolf Gustavsson[2], Jan-Olov Aidanpää[1]

ISROMAC 2016

International Symposium on Transport Phenomena and Dynamics of Rotating Machinery

Hawaii, Honolulu

April 10-15, 2016

Abstract

In vertically oriented machines with tilting-pad journal bearings, there is no static load that allow to calculate the bearing properties around a determined static position. As a result, most of simulations are performed by solving Reynolds equation at each time-step which can result in long computational time. To avoid this concern, a simplified model is used that takes in account the variation of unbalance load depending on the pad configuration. This nonlinear model is used to simulate the dynamics of a hydropower turbine and compared with the Campbell diagram calculations used from hydropower industry standards. A comparison between the linear and nonlinear model is performed to evaluate how accurate the linear model is and until which limits it can be relevant. In case of qualitative discrepancies in the results in terms of natural frequencies and damping ratios, an improvement of the Campbell diagram calculation is proposed to obtain a more accurate linear model.

Keywords

Hydropower — Tilting-pad — Vertical machine

[1] *Department of Engineering Sciences and Mathematics, Luleå University of Technology, Luleå, Sweden*

[2] *Vattenfall Research AB, Älvkarleby, Sweden*

***Corresponding author**: florian.thiery@ltu.se

INTRODUCTION

In usual horizontal turbomachines, the dynamical properties of the system are calculated around the static load due to dead weight. On the contrary, for vertical machines such as pumps and hydropower turbines, the rotor is subjected to rotating unbalance loads that do not allow to calculate constant stiffness and damping coefficients for fixed operating conditions. Instead, the bearing forces depend on the relative displacements and velocities between the shaft and housing. As a result, the Reynolds equation is usually solved at each time step and the Campbell diagram is not available anymore due to the nonlinear equations of motion [1–5]. The main problem of solving Reynolds equation at each time-step resides in the long computational time especially when performing a design study as function of several design parameters and/or different unbalance loads. As a result, it is convenient to simplify the bearing modeling without losing the mechanical properties of the system and perform nonlinear simulations using the simpler model.

However, from an industrial point of view, it is desirable - as a first step - to obtain the Campbell diagram to evaluate critical designs for hydropower rotors. As a result, a first evaluation can be performed by assuming the bearing loads to be constant at each bearing position as it is usually done for horizontal machines. A comparison

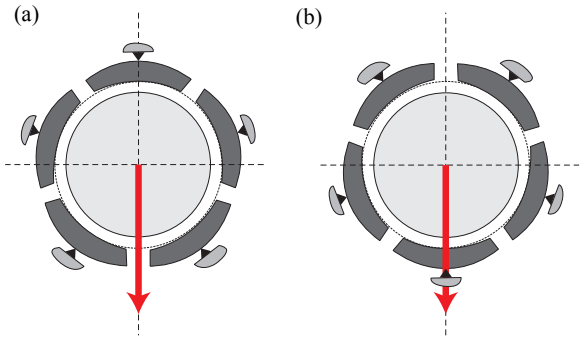

Figure 1. Tilting pad bearing configuration: (a) Load-Between-Pad (b) Load-On-Pad

with the frequency content of the sweep sine for the nonlinear equation of motion is performed to investigate to which extent is this assumption valid. The nonlinear model used in this paper is simplified by assuming a harmonic variation of the bearing coefficients as function of the number of pads that takes in account the variation of stiffness and damping between the Load-On-Pad (LOP) and Load-Between-Pad (LBP) configuration (see Fig .1) If the comparison between the linear and nonlinear is unsatisfactory, a strategy to upgrade the Campbell diagram should be determined to evaluate in a correct

NOMENCLATURE

Roman Symbols

a_k	coefficients of bearing polynoms
c_{ij}	bearing damping coefficient
e	unbalance eccentricity
f_0	start frequency sweep sine
f_{asyn}	asynchronous force
f_{unb}	unbalance force
f_e	end frequency sweep sine
J_d	diametrical moment of inertia
J_p	polar moment of inertia
k_{UMP}	magnetic pull stiffness
k_{ij}	bearing stiffness coefficient
m	disk mass
N_{pads}	number of tilting pads
q	state space vector
t_f	total simulation time
x, y	displacement in fixed coordinate system

Bold symbols

$\mathbf{C_{bear}}$	bearing damping matrix
$\mathbf{C}$	damping matrix
$\mathbf{G}$	gyroscopic matrix
$\mathbf{I}$	identity matrix
$\mathbf{K_{bear}}$	bearing stiffness matrix
$\mathbf{K}$	stiffness matrix
$\mathbf{M}$	mass matrix
$\mathbf{T}$	transformation matrix

Greek Symbols

Ω	rotating speed
Ω_{nom}	nominal speed
ε	eccentricity
φ	load angle
ξ, η	displacement in rotating coordinate system

Acronym

G	balancing grade
LBP	load-between-pad
LGB	lower guide bearing
LOP	load-on-pad
TGB	turbine guide bearing
UGB	upper guide bearing
UMP	unbalance magnetic pull

way the natural frequencies and damping ratios of the system.

1. METHODS

1.1 Model

1.1.1 Rotor description

The model of the vertical hydropower unit used in this paper is a typical 45MW Kaplan turbine [6] as seen in Fig.2. The rotor is supported by three tilting pad journal bearings at the upper guide bearing (UGB), the lower guide bearing (LGB) and the turbine guide bearing (TGB). The shaft is described using Timoshenko beam elements, while additional mass and inertia properties are added at the exciter, generator and runner position. The Unbalance Magnetic Pull is simulated as a constant negative stiffness at the generator and exciter position. The values of these parameters are summarized in Table 2. The rotor is at first described using 15 nodes, but it is reduced to 6 nodes using the Improved Reduction System method [7]. The 6 master nodes kept for the simulation are the three bearing positions as well as the exciter, the generator and runner position.

1.1.2 Bearings modeling

The generator is set vertically and supported by tilting pad journal bearings (TPJB) that are attached to rigid bearing brackets on each side. The bearings will be considered to have a nonlinear behavior. Since the rotor is vertical, there is no static load caused by the dead weight that allows the calculation of bearing coefficients. In fact, the stiffness and bearing properties of the system will depend on the load direction. These coefficients will be determined as function of the Load on Pad (LOP) or Load between Pad (LBP) (Fig.1), load angle φ and eccentricity ε. The tilting pad bearings are oriented in a way that the between-pad area is aligned with the y-direction in all three positions in Fig. 2. The calculation of bearing coefficients follows the procedure of [8]. Using the parameters in Table 2, a commercial software [9] is used to calculate the bearings for both LOP and LBP as function of the eccentricity. These coefficients can be approximated using eccentricity dependent polynomial functions. For instance, the stiffness coefficient in ξ-direction is $k_{\xi}^{\text{LOP}} = a_0 + a_1\varepsilon + a_2\varepsilon^2 + a_3\varepsilon^3 + a_4\varepsilon^4$ where ε is the eccentricity. The stiffness and damping coefficients in the rotating system are then assumed to be a harmonic relation of the LOP, LBP and load angle φ as follows:

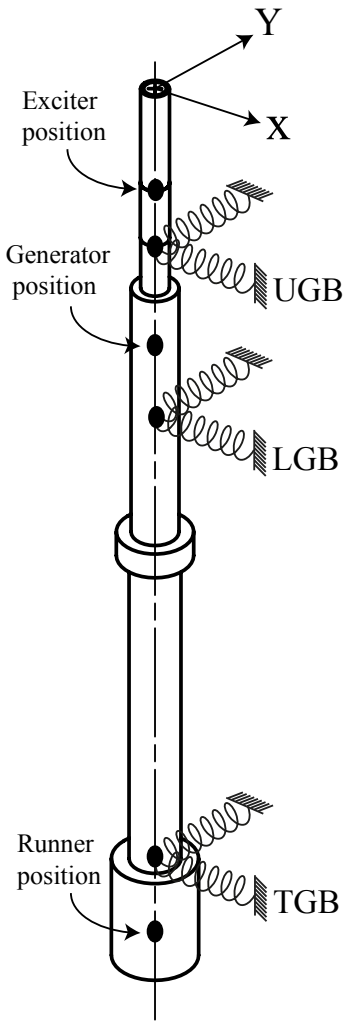

Figure 2. Model of a 45 MW hydropower turbine. The generator and runner are not graphically shown, but mass and inertias are set in the model in agreement with their geometry

$$k_{ij} = \frac{\Omega}{\Omega_{\text{nom}}}\left(\frac{k_{ij}^{\text{LOP}} + k_{ij}^{\text{LBP}}}{2} + \frac{k_{ij}^{\text{LOP}} - k_{ij}^{\text{LBP}}}{2}\cos(N_{\text{pads}}\varphi)\right) \quad (1)$$

$$c_{ij} = \frac{c_{ij}^{\text{LOP}} + c_{ij}^{\text{LBP}}}{2} + \frac{c_{ij}^{\text{LOP}} - c_{ij}^{\text{LBP}}}{2}\cos(N_{\text{pads}}\varphi) \quad (2)$$

where $i, j = \xi, \eta$.The stiffness coefficients are scaled with the nominal speed used for their calculation, whereas the damping coefficents are constant as function of the rotating speed. Fig.3 shows a representation of direct stiffness and damping as function of eccentricity, calculated at the nominal speed of 166.7 RPM. In this model, the cross-coupling terms are disregarded due to their small values. Moreover, the mass parameters of the fluid are also neglected due to small forces. Since the bearing properties are given in the rotating $\xi\eta$-plane following the unbalance load, they have to be transformed to the fixed coordinate system using the following transformation matrix

$$\mathbf{T} = \begin{pmatrix} \cos(\varphi) & \sin(\varphi) \\ -\sin(\varphi) & \cos(\varphi) \end{pmatrix} \quad (3)$$

where $\varphi = \arctan(y/x) + n\pi$ is the eccentricity angle at the corresponding bearing position. As a result, the bearing matrices are transformed at each time step using $\mathbf{K}_{\text{bear}} = \mathbf{T}^\top \mathbf{K}_{\text{rot}} \mathbf{T}$ and $\mathbf{C}_{\text{bear}} = \mathbf{T}^\top \mathbf{C}_{\text{rot}} \mathbf{T}$. The parameters for each bearing position are given in Table 1 to obtain the bearing stiffness and damping using Eq. 2.

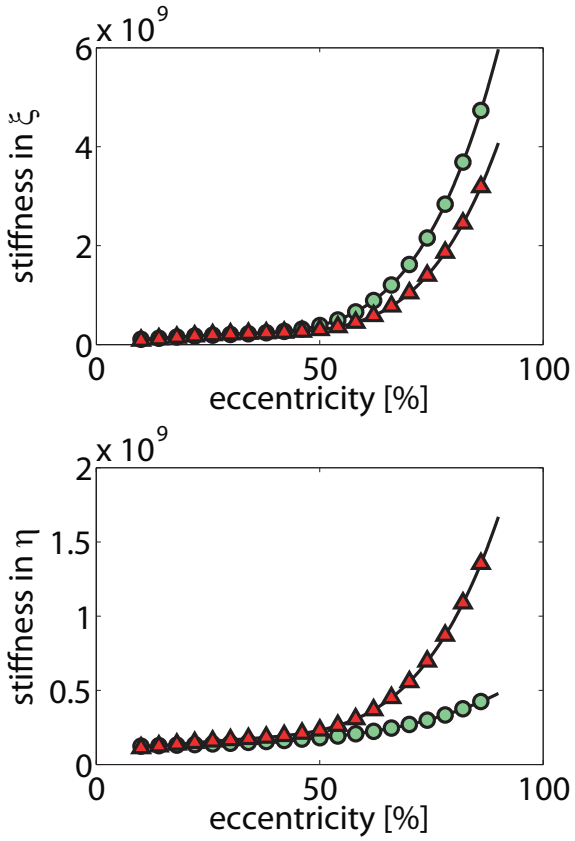

Figure 3. Direct stiffness of the bearing in the local coordinate system rotating with the load. (△) represents the Load-Between-Pad stiffness and (○) is the Load-On-Pad stiffness

Table 1. Bearing coefficients

Bearing Properties	Value	Coefficient	a_0	a_1	a_2	a_3	a_4
Position	Upper Guide	k_ξ^{LOP}	0.1×10^9	-0.5082×10^7	0.8322×10^6	-0.2702×10^5	0.2939×10^3
Clearance	0.2×10^{-3}	k_ξ^{LBP}	0.5×10^8	-0.2303×10^7	0.7955×10^6	-0.2546×10^5	0.2492×10^3
Number pads	6	k_η^{LOP}	0.12×10^9	0.4806×10^5	0.4032×10^5	-0.8151×10^3	0.9483×10^1
Speed	166.67 RPM	k_η^{LBP}	0.9×10^8	0.9406×10^6	0.18502×10^6	-0.6631×10^4	0.7361×10^2
		c_ξ^{LOP}	0.55×10^7	-0.4202×10^5	0.1995×10^5	-0.69×10^3	0.8121×10^1
		c_ξ^{LBP}	0.6×10^7	-0.2151×10^6	0.2896×10^5	-0.8074×10^3	0.7667×10^1
		c_η^{LOP}	0.69×10^7	-0.1545×10^5	0.2070×10^4	-0.3166×10^2	0.3246×10^0
		c_η^{LBP}	0.6×10^7	0.1455×10^5	0.6282×10^4	-0.2002×10^3	0.2250×10^1
Position	Lower Guide	k_ξ^{LOP}	0.83×10^9	-0.804×10^8	0.786×10^7	-0.2150×10^6	0.196×10^4
Clearance	0.175×10^{-3}	k_ξ^{LBP}	0.6×10^9	-0.6689×10^8	0.871×10^7	-0.2468×10^6	0.2207×10^4
Number pads	24	k_η^{LOP}	0.75×10^9	-0.486×10^7	0.305×10^6	-0.477×10^4	0.545×10^2
Speed	166.67 RPM	k_η^{LBP}	0.67×10^9	0.446×10^7	0.269×10^6	-0.954×10^4	0.112×10^3
		c_ξ^{LOP}	0.19×10^8	-0.114×10^7	0.127×10^6	-0.387×10^4	0.40×10^2
		c_ξ^{LBP}	0.20×10^7	-0.6407×10^6	0.1727×10^6	-0.5473×10^4	0.5271×10^2
		c_η^{LOP}	0.17×10^8	-0.961×10^5	0.60×10^4	-0.943×10^2	0.109×10^1
		c_η^{LBP}	0.14×10^8	0.221×10^6	0.223×10^4	$/0.181 \times 10^3$	0.248×10^1
Position	Turbine Guide	k_ξ^{LOP}	0.3×10^9	-0.161×10^8	0.249×10^7	-0.7955×10^5	0.8579×10^3
Clearance	0.175×10^{-3}	k_ξ^{LBP}	0.34×10^9	-0.1275×10^8	0.1751×10^7	-0.5343×10^5	0.5858×10^3
Number pads	8	k_η^{LOP}	0.3×10^9	0.506×10^7	0.1547×10^5	-0.2881×10^4	0.5237×10^2
Speed	166.67 RPM	k_η^{LBP}	0.31×10^9	0.301×10^7	0.219×10^6	-0.955×10^4	0.135×10^3
		c_ξ^{LOP}	0.15×10^8	-0.5099×10^6	0.6172×10^5	-0.1796×10^4	0.1923×10^2
		c_ξ^{LBP}	0.12×10^8	0.9974×10^5	0.2266×10^5	-0.8552×10^3	0.1122×10^2
		c_η^{LOP}	0.15×10^8	-0.607×10^5	0.783×10^4	-0.169×10^3	0.178×10^1
		c_η^{LBP}	0.14×10^8	0.522×10^5	0.621×10^4	-0.219×10^3	0.312×10^1

1.1.3 Unbalance loads configuration

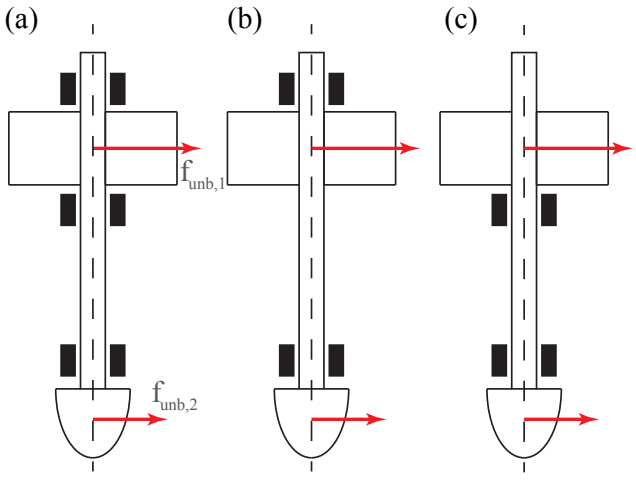

Figure 4. Bearing configuration for different hydropower machines (a) UGB, LGB, and TGB (b) UGB and TGB (c) LGB and TGB

To perform rotordynamical simulations, international standards from hydropower industry have to be estimated regarding unbalance and eccentricities. First of all, the ISO 1940-1 [10] standard gives recommendation concerning the maximum allowed unbalance force which is dependent on the rotating mass, rotationnal speed and balancing grade. The balancing grade for hydropower rotors is G6.3, meaning that $e\Omega = 6.3$ mm/s. The maximum allowed unbalance force is thus defined as

$$f_{\text{unb}} = m \times (e\Omega) \times \Omega = m \times (\frac{6.3}{1000}) \times \Omega \qquad (4)$$

where m represents the mass from Table 2 at the corresponding position. According to Fig. 4, the unbalance loads are reasonably assumed to be set at the generator and runner position. The distribution of the unbalance forces depend on the bearing layout in the machine. In our case, the configuration corresponds to Fig. 4(a) with a 3 bearings unit. By assuming the rotor to be rigid in comparison with the bearing stiffness, the unbalance load from the generator will be distributed between the

two generator bearings, while the entire unbalance load from the runner will be on the turbine bearing.

1.2 Simulation procedure

1.2.1 Linear case - Campbell diagram

For calculation of the Campbell diagram, several assumptions have to be made. First of all, the stiffness and damping properties are calculated with the LOP configuration. Secondly, the load is considered static - similarly to horizontal machines - so that the bearing properties are fixed in the global coordinate system. Finally, the unbalance load is assumed to be defined by Eq. 4 at the generator and runner position. By knowing the unbalance positions, the bearing configuration and assuming the rotor to be rigid, the calculation of the stiffness and damping coefficients can be performed for each bearing by increasing the speed (and simultaneously the unbalance load) as the bearing load is known. In order to investigate more deeply the structural properties of the turbine, another evaluation of the Campbell diagram is performed at the operational speed as function of the bearing load. Since there is always uncertainties regarding the unbalance load, this diagram should help understand the global behavour of the machine.

1.2.2 Nonlinear case - sweep sine

In this section, the full nonlinear modeling is used to investigate the vibration properties of the system. The stiffness and damping properties are calculated for each bearing using Eq. 2 and Table 1 at each time step as function of load angle, eccentricity and speed using the following equation of motion in state space formulation:

$$\dot{\mathbf{q}} = \begin{bmatrix} \mathbf{0} & \mathbf{I} \\ -\mathbf{M}^{-1}\mathbf{K} & -\mathbf{M}^{-1}(\Omega\mathbf{G} + \mathbf{C}) \end{bmatrix} \mathbf{q} + \begin{bmatrix} \mathbf{0} \\ -\mathbf{M}^{-1}(\mathbf{f}_{\text{unb}} + \mathbf{f}_{\text{asyn}}) \end{bmatrix} \quad (5)$$

where $\mathbf{M}$ is the consistent mass matrix, $\mathbf{C}$ the damping matrix containing only the damping properties of the bearings, $\mathbf{G}$ the gyroscopic matrix and $\mathbf{K}$ the stiffness matrix which is updated at each time-step due to variation of eccentricity and load angle. Eq.(5) is solved using the 4th order Runge-Kutta-Fehlberg (RKF) method with adaptive time-step. The unbalance is assumed the same as for the calculation of the Campbell diagram. To investigate the vibration response of the system, another simulation is performed where an additional asynchronous force is added at the runner position with a linear sweep-sine excitation of the form

$$f_{\text{asyn}} = 0.01 f_{\text{unb}} \cos(2\pi f_0 t + 2\pi \frac{f_e - f_0}{t_f} t^2) \quad (6)$$

The magnitude of the force is 1% of the unbalance load in order to keep the same bearing properties. f_0 and f_e represents respectively the starting and ending frequency of the sweep sine, and t_f is the total simulation time. To obtain the resonance frequencies from the nonlinear case, the response signal with unbalance force only is subtracted to the response signal with unbalance and sweep sine forces. Moreover, a forward and a backward sweep sine simulations are performed to distinguish between the forward and backward modes as they are close to each another for this particular turbine.

2. RESULTS AND DISCUSSION

2.1 Linear analysis

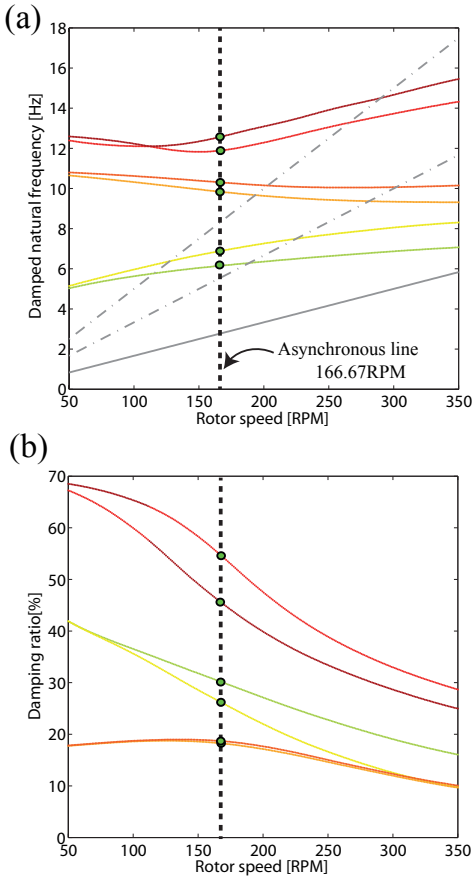

Figure 5. Damped natural frequency and damping ratios of the first six modes of vibration as function of the rotating speed

Table 2. Mechanical properties of the Forsmo turbine

Symbol	Item	Runner	Rotor	Exciter
m	mass [kg]	65170	197200	2800
J_d	diametrical moment of inertia [kg.m^2]	60055	566500	0
J_p	polar moment of inertia [kg.m^2]	104800	1133000	0
		Turbine guide bearing	Lower guide bearing	Upper guide bearing
k_{UMP}	Magnetic stiffness [N/m]	X	-310×10^6	-7.6×10^6

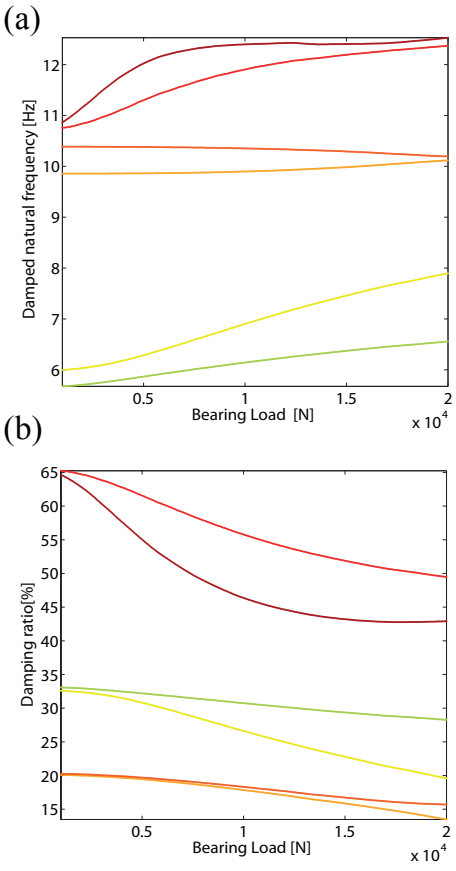

Figure 6. Damped natural frequency and damping ratios of the first six modes of vibration as function of the bearing load at the speed of 166.67 RPM

The Campbell diagram as function of the rotating speed and an eccentricity $e = 0.63 \times 10^{-3} m$ at the generator and runner position is displayed in Fig.5. First of all, it should be noted that the modes of vibration with more than 90 % damping ratio are disregarded. It can be observed that the damped natural frequencies of the system are close to each other, and the damping ratios of the system are high especially for the third mode of vibration. The values of damped natural frequency and damping ratios are given in Table 3 for comparison

Table 3. Modal properties of the turbine at Ω = 166.67 RPM

Mode of vibration	Damped natural frequency [Hz]	Damping ratio [%]
Mode 1	6.15	30.22
Mode 2	6.89	26.27
Mode 3	9.84	18.26
Mode 4	10.30	18.70
Mode 5	11.89	54.78
Mode 6	12.58	45.69

purposes with the nonlinear case. Fig. 6 shows the Campbell diagram as function of the bearing load for a speed of 166.67 RPM by assuming that the load is equal in all the bearings. The variation of bearing load slightly influences the first mode of vibration of the entire range and the third mode of vibration for a bearing load $\leq$ 15 kN. The second mode of vibration stay constant compared with the two other modes have increasing frequencies. Additional information concerning the modes of vibration is available in Fig. 7. It can be observed that mode 1-2 and 5-6 correspond to a generator mode while mode 3-4 is related with the runner displacement.

2.2 Nonlinear analysis

The maximum displacement at the runner is displayed as function of the instantaneous frequency in Fig. 8 with the asynchronous excitation at the runner position as well. The black curve represents the response under a forward excitation, while the red curve represents backward excitation. It should be noted that the forward and backward property is specific to a node position and can be different in another node position. The response shows higher vibrations at 10.42 Hz and 10.89 Hz and lower vibrations around 9.15 Hz and 9.39 Hz.

Fig. 9 shows the response at the runner position with an asynchronous force at the generator position. Similarly, higher vibrations appear at 9.31 Hz and 10.37

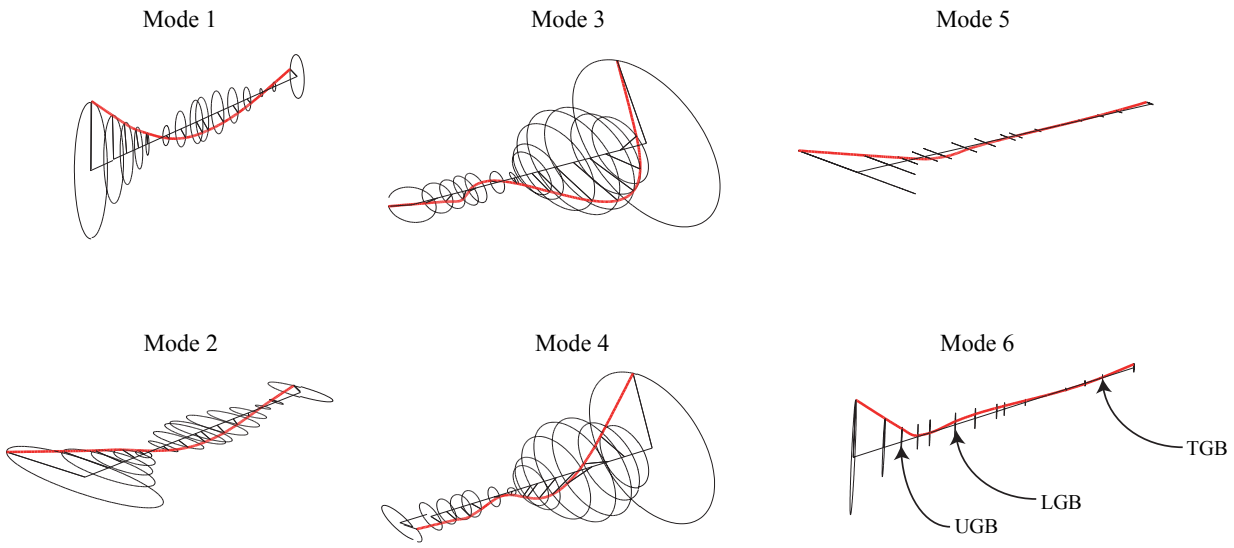

Figure 7. Modes of vibration of the Forsmo turbine. The bearing positions are shown in mode 6 and are the same for the other modes

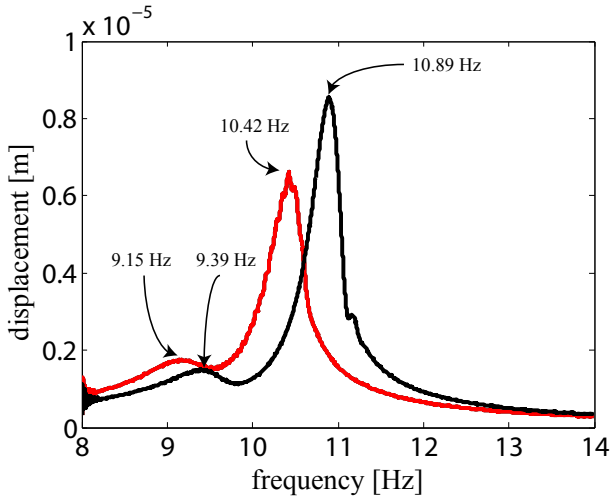

Figure 8. Envelope of the displacement at the runner position under a sweep sine excitation at the runner position

Hz (backward) as well as 9.50 Hz and 10.80 Hz (forward). In the Campbell diagram displayed in Fig. 5, the 6 modes of vibration should be observed as they cross the asynchronous line. However, only 4 peaks are visible in the sweep sine excitation responses. It is reasonable to assume that mode 3 and 4 correspond to the 3rd and 4th peak response since they have the higher amplitude (lower damping ratios), close frequencies (< 10 % error) and the runner displacement is greater as compared with other nodal positions which correlates the mode of vibration shown in Fig. 7. Concerning the 1st and 2nd peak response, it can also be assumed that it corresponds to mode 1 and mode 2 even as the damping ratios are greater than mode 3 and 4. However, the Campbell diagram predicts damped natural frequencies of 6.15 Hz and 6.89 Hz that are far away from the nonlinear simulation. Another major difference with the linear case is the absence of vibration for mode 5 and 6 in the studied range. However, this may be due to the high damping ratios of the corresponding modes that suppress the vibrations.

CONCLUSION

The nonlinear simulation of a hydropower turbine has been performed in this article. The model used here has some advantages since it allows to perform fast simulations by using simplified bearing calculations based on the assumption of harmonic stiffness and damping due to variation between LOP and LBP configuration specific to vertical machines. Due to the variation of stiffness during operation, the Campbell diagram calculated in hydropower industry may not be accurate as several assumptions are done in order to calculate the eigenfrequencies and damping ratios. For instance, it was shown that the assumption of constant stiffness with LOP configuration allowed to calculate accurately the 3rd and 4th mode of vibration, but it underestimated the

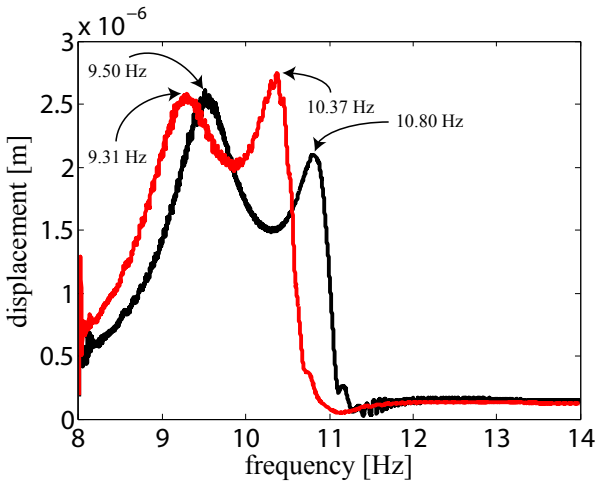

Figure 9. Envelope of the displacement at the runner position under a sweep sine excitation at the generator position

first two natural frequencies of the system. One of the main problem when calculating the modal properties is the assumption of equivalent load at each bearing. Even though it is true for this bearing configuration and by assuming a rigid rotor, it becomes unclear to know what is the bearing load distribution when the rotating speed is increased. One of a solution to improve the Campbell diagram is to perform the nonlinear simulation at all speeds and retrieve the average bearing load at steady state in order to use it back to calculate a more accurate Campbell diagram. However, this method is not practical since it involves a great number of simulations, but it would be a better solution to improve accuracy in the linear study. Another suggestion would be to use Floquet theory as long as the variation of stiffness and damping is periodic at steady-state.

ACKNOWLEDGMENTS

The research presented was carried out as a part of "Swedish Hydropower Centre - SVC". SVC has been established by the Swedish Energy Agency, Elforsk and Svenska Kraftnät together with Luleå University of Technology, The Royal Institute of Technology, Chalmers University of Technology and Uppsala University. www.svc.nu.

REFERENCES

[1] Maurice F White, Erik Torbergsen, and Victor A Lumpkin. Rotordynamic analysis of a vertical pump with tilting-pad journal bearings. *Wear*, 207(1–2):128 – 136, 1997.

[2] Li-Feng Ma and Xin-Zhi Zhang. Numerical simulation of nonlinear oil film forces of tilting-pad guide bearing in large hydro-unit. *International Journal of Rotating Machinery*, 6(5):345–353, 2000.

[3] Zhang Y.b Ji L.a Wu Y.c Yu Y.a Yu L.d Lü, Y.a. Analysis of nonlinear dynamic behaviors of rotor system supported by tilting-pad journal bearings. *Zhendong Ceshi Yu Zhenduan/Journal of Vibration, Measurement and Diagnosis*, 30(5):539–543, 2010.

[4] R. Cardinali, R. Nordmann, and A. Sperber. *Mechanical Systems and Signal Processing*, 7(1):29 – 44, 1993.

[5] Matthew Cha and Sergei Glavatskih. Nonlinear dynamic behaviour of vertical and horizontal rotors in compliant liner tilting pad journal bearings: Some design considerations. *Tribology International*, 82, Part A:142 – 152, 2015.

[6] Erik Synnegård, Rolf K. Gustavsson, and Jan-Olov Aidanpää. *Modeling of visco-elastic supports for hydropower applications*, volume XVIII of *Mechanisms and Machine Science*, pages 2189–2197. Springer, 2015.

[7] F. Thiery, R. Gustavsson, and J.O. Aidanpaa. Dynamics of a misaligned kaplan turbine with blade-to-stator contacts. *International Journal of Mechanical Sciences*, 99:251–261, 2015.

[8] Mattias Nässelqvist, Rolf Gustavsson, and Jan-Olov Aidanpää. Experimental and numerical simulation of unbalance response in vertical test rig with tilting-pad bearings. *International Journal of Rotating Machinery*, 2014:10, 2014.

[9] Rotordynamics and Seal Research. Rappid.

[10] Swedish Standards Institute. Ss-iso 1940-1 : Mechanical vibration - balance quality requirements for rotors in a constant (rigid) state - part 1: Specification and verification of balance tolerances. Technical report, ed. Stockholm: SIS Forlag AB, 2003.